Nano Energy (2014) 9, 80–87

Available online at www.sciencedirect.com

ScienceDirect

journal homepage: www.elsevier.com/locate/nanoenergy

RAPID COMMUNICATION

Symbiotic $CeH_{2.73}/CeO_2$ catalyst: A novel hydrogen pump

Huai-Jun Lin[a,d], Jia-Jun Tang[a,c], Qian Yu[b,e,*], Hui Wang[a], Liu-Zhang Ouyang[a], Yu-Jun Zhao[c], Jiang-Wen Liu[a], Wei-Hua Wang[d,**], Min Zhu[a,***]

[a]*School of Materials Science and Engineering, South China University of Technology, Key Laboratory of Advanced Energy Storage Materials of Guangdong Province, Guangzhou 510640, PR China*
[b]*National Center for Electron Microscopy, Lawrence Berkeley National Laboratory, Berkeley, CA 94720, United States*
[c]*Department of Physics, South China University of Technology, Guangzhou 510640, PR China*
[d]*Institute of Physics, Chinese Academy of Sciences, Beijing 100080, PR China*
[e]*Center of Electron Microscopy and State Key Laboratory of Silicon Materials, Department of Materials Science and Engineering, Zhejiang University, Hangzhou 310027, PR China*

Received 14 April 2014; received in revised form 16 June 2014; accepted 24 June 2014
Available online 15 July 2014

KEYWORDS
Hydrogen storage;
MgH_2;
Symbiotic $CeH_{2.73}/CeO_2$;
Catalysis;
In situ HRTEM;
Theoretical calculations

Abstract
Using additives/catalysts to destabilize hydrides of high hydrogen storage density, *e.g.* MgH_2 with 7.6 wt%-H and desorption temperature as high as 300–400 °C, is one of the most important strategies to overcome the hurdle of applying hydrogen storage materials in technologies related to hydrogen energy. Despite tremendous efforts, to develop additives/catalysts with high catalytic activity and easy doping remains a great challenge. Here, we report a simple method to induce a novel symbiotic $CeH_{2.73}/CeO_2$ catalyst in Mg-based hydrides, which is capable of massive fabrication. More importantly, we reveal a spontaneous hydrogen release effect at the $CeH_{2.73}/CeO_2$ interface, which leads to dramatic increase of catalysis than either sole $CeH_{2.73}$ or CeO_2 catalyst. Maximum hydrogen desorption temperature reduction of MgH_2 could reach down to ~210 °C as molar ratio of $CeH_{2.73}$ to CeO_2 was 1:1. The dynamic boundary evolution during hydrogen desorption was observed in the symbiotic $CeH_{2.73}/CeO_2$ at atomic resolution using *in situ* High-Resolution Transmission Electron Microscope (HRTEM). Combining the *ab-initio* calculations, which show significant reduction of the formation energy of V_H (hydrogen vacancy) in the $CeH_{2.73}/CeO_2$ boundary region in comparison to those in the bulk

*Corresponding author at: National Center for Electron Microscopy, Lawrence Berkeley National Laboratory, Berkeley, CA 94720, United States.
**Corresponding author.
***Corresponding author.
E-mail addresses: qyu@lbl.gov (Q. Yu), whw@iphy.ac.cn (W.-H. Wang), memzhu@scut.edu.cn (M. Zhu).

http://dx.doi.org/10.1016/j.nanoen.2014.06.026

MgH_2 and $CeH_{2.73}$, we demonstrate that the outstanding catalytic activity can be attributed to the spontaneous hydrogen release effect at the $CeH_{2.73}/CeO_2$ interface.

Introduction

Hydrogen, as an ideal fuel for future clean and renewable energy system, will hardly be practically applied if it could not be safely stored in appropriate way [1-3]. Solid-state hydrogen storage materials, *e.g.* MgH_2 with hydrogen storage density of ~7.6 wt%, are widely considered as promising carriers for hydrogen storage. However, temperature as high as 300-400 °C is generally required for desorption of MgH_2 due to the stable thermodynamics and sluggish kinetics [4]. Therefore, exploring advanced catalysts plays important role for the development of high capacity hydrogen storage materials. Catalysts doping by methods of ball milling and chemical process, very often together with nanoscaling, is a vital way to compensate the kinetic drawbacks [5]. Transition metals [6], chlorides [7], hydrides [8] and oxides [9,10] *etc*. have been found to present catalytic activity for de/hydrogenation of Mg-based materials, which might be driven from the "hydrogen spillover" effect [11,12], electron transfer of the high-valence cations [13,14], formation of anion-containing species [7] or MgH_2-catalysts interface reaction [15] *etc*. Direct evidence is highly demanded to clarify and understand the intrinsic catalysis, which is unfortunately not available so far.

Another critical issue raised is in the practical doping process of catalysts in hydrogen storage materials. Generally speaking, sophisticated chemical synthesis process and ball milling are commonly adopted. Although the former one can lead to excellent de/hydrogenation kinetics, it is usually not suitable for massive production plus the requirement of extra treatment for polluted chemical agents [16,17], while the later one is also associated with the difficulty of the control of size and distribution of the catalysts. In addition, contamination harmful to materials is easily induced by atmosphere and milling debris in the long-time process. Therefore, to develop easy and effective doping strategy of catalyst, capable of massive fabrication in the hydrogen storage materials with well-controlled structure and distribution is crucial for optimal catalyzing effect and presumably has strong impact on the practical application of catalysts doped hydrogen storage materials.

In this work, we propose a simple strategy to generate a novel symbiotic $CeH_{2.73}/CeO_2$ catalyst in Mg-based hydrides with controlled size by simple conventional hydriding and heat treatment process exempting long-time ball milling and sophisticated chemical process. *In situ* HRTEM characterizations during dehydrogenation were performed together with *ab-initio* calculations to reveal the catalysis. A spontaneous hydrogen release effect (corresponding to negative formation energy of V_H) in the $CeH_{2.73}/CeO_2$ interface is responsible for the improvement of the dehydrogenation of MgH_2.

Experimental details

Materials synthesis

Preparation details of the amorphous Mg-Ce-Ni ribbons are described elsewhere [18,19]. The amorphous ribbons with composition of $Mg_{80}Ce_{10}Ni_{10}$ were crushed *via* ball milling (200 rpm) for only 2 h into powder, and then screened through 200 mesh sieves. After that, the powder was thermally activated under hydrogen gas of 10 MPa at 300 °C for 3 h and then treated by 15 times dehydrogenated and rehydrogenated at 300 °C for 0.5 h under 0.02 and 3 MPa hydrogen gas, respectively. Then, the 15th cycled sample was placed in an Ar-atmosphere glove box for around 1 week (passivation treatment). Finally, about 0.30 g sample was sealed in a tube (2 ml) full of air at room temperature for 1, 5, 8 and 20 h to obtain the MgH_2-Mg_2NiH_4-$CeH_{2.73}/CeO_2$ nanocomposites with different molar ratios of CeO_2 to $CeH_{2.73}$.

Characterizations

Common phase analysis and *in situ* high-temperature X-ray diffraction (XRD) analysis were conducted on a Philips X'Pert MPD X-ray diffractometer with Cu Kα radiation. Conventional transmission electron microscopy (TEM) and high resolution transmission electron microscopy (HRTEM) observations were carried out on a JEOL JEM-2100 microscopy with 200 kV voltage. The *in situ* TEM measurements were performed in a TECNAI microscopes with the Gatan heating holders. The samples were heated up to about 300 °C. The electron beam heating also contributes to the increase of temperature. Scherzer resolution of the TECNAI is 0.19 nm, and information limit is 0.12 nm. Differential scanning calorimetry (DSC) tests were carried out on a Netzsch STA-409 analyzer; the separation (peak deconvolution) was done using the PeakFit 4.12 software with a Gaussian response function. TPD-MS analysis was performed on a Hiden Qic-20 mass spectrometer. Hydrogenation/dehydrogenation kinetics and cycles tests were performed on a Sieverts-type automatic gas reaction controller (Pct Pro2000). The sample weight for hydrogen storage property test was around 100 mg.

Theoretical calculations

Our theoretical calculations were performed using Vienna *ab initio* Simulation Package [20-22]. We applied the spin-polarized density-functional theory (DFT) in the DFT+*U* approach (*U* is a Hubbard-like term describing the onsite Coulomb interactions) with the PBE (Perdew-Burke-Ernzerhof) functional [23] and projector-augmented wave (PAW) potentials [24]. For cerium and oxygen atoms, the (5*s*, 5*p*, 6*s*, 4*f*,

5*d*) and (2*s*, 2*p*) states were treated as valence electrons. In the DFT+*U* calculations, the U_{eff} value [25] of 5.00 eV was used. In all the calculations, adequate tests with k-points meshes [26] were done to show excellent converged results with energy convergence to be in precision of ~0.001 eV per cell and the plane-wave cutoff energy was set to be 400 eV. The internal optimization was converged with the force on each atom to be less than 0.01 eV/Å. The $CeH_x(111)/CeO_2(111)$ (x=2, 2.25, 2.5, 2.75 and 3) interfaces were modeled using a supercell containing two phases where each phase with three layers (shown in Figure 4c). The calculated CeO_2, CeH_2, $CeH_{2.75}$ and CeO_3 bulk equilibrium lattice constant were 5.492 Å, 5.415 Å, 5.507 Å and 5.429 Å, respectively. Considering slight differences between these lattice constants, we built a (2 × 2) coherent interface model, with 24 cerium atoms, 24 oxygen atoms and 12x hydrogen atoms (x=2, 2.25, 2.5, 2.75 and 3) and lattice constants of 5.51 Å. Test calculations indicated that convergence problem occurred when the interface model was with vacuum. Therefore, the model was built having two identical interfaces without vacuum. All atoms in models were allowed to relax with the interface unit cell kept fixed during geometry optimization.

Results and discussion

Materials synthesis

The process of inducing symbiotic $CeH_{2.73}/CeO_2$ catalyst in the MgH_2 matrix is shown in Figure 1. The first step is to hydrogenate the amorphous Mg-Ce-Ni alloy (Figure 1a) to get a multiphase composite of MgH_2, Mg_2NiH_4 and $CeH_{2.73}$ (Figure 1b). The second step is to oxidize the hydrogenated sample to generate CeO_2 from $CeH_{2.73}$ (Figure 1c). The transition process of the microstructure in the above treatment process is revealed by the X-ray diffraction (XRD) analyses, which are shown in the insets of Figure 1. The CeO_2 is formed from $CeH_{2.73}$ and the molar ratio of CeO_2 to $CeH_{2.73}$ could be determined by oxidation process. The ratio is ~1:1 in the situation of ~8 h oxidation at 25 °C. It is significant that Gibbs free energy ΔG of the reaction $CeH_{2.73}+O_2 \rightarrow CeO_2+H_2$ at 25 °C is −1423 kJ while that of the reaction $MgH_2+O_2 \rightarrow MgO+H_2$ at 25 °C is −1066 kJ [27]. Thus, only CeO_2 could be induced with exclusion of MgO formation under suitable control of oxidation process.

In order to reveal the structural relationship between $CeH_{2.73}$ and CeO_2, TEM and HRTEM observations are performed as shown in Figure 2. Figure 2a shows the HRTEM image of the typical symbiotic structure of the $CeO_2/CeH_{2.73}$ nanoparticles, and they can also form core-shell structure as shown in Figure 2b and c. Since the lattice parameters of $CeH_{2.73}$ (space group: *Fm*-3*m*, a=0.5530 nm, PDF 89-3694) and CeO_2 (space group: *Fm*-3*m*, a=0.5412 nm, PDF 81-0792) are extremely close, we performed HRTEM images, FFT patterns and also EDS analysis to confirm that CeO_2 was epitaxially formed from $CeH_{2.73}$ in a cubic to cubic orientation relationship. More microstructural characterizations for the MgH_2-Mg_2NiH_4-$CeH_{2.73}/CeO_2$ composite are given in Figures S1 and S2.

Hydrogen desorption

The MgH_2-Mg_2NiH_4-$CeH_{2.73}/CeO_2$ composite displays remarkable reduction of hydrogen desorption temperature compared with that of the conventional MgH_2. It is important to note that this is highly related to the ratio of $CeH_{2.73}$ to CeO_2 (Figure S3). With the increase of that ratio, the hydrogen desorption temperature decreases at first and then increases after reaching the trough at the molar ratio of 1:1. We suppose that the catalytic activity of the symbiotic $CeH_{2.73}/CeO_2$ might have close relationship with their interface density, which reaches the maximum when molar ratio of $CeH_{2.73}$ to CeO_2 is 1:1, however, the mechanism is not well understood. The lowest dehydrogenation onset temperature, as determined by DSC measurement, is only ~210 °C at the presence of the symbiotic $CeH_{2.73}/CeO_2$, which is ~210 °C lower than that of conventional MgH_2 (Figure 3a). In order to reveal the detailed evolution of phases of the MgH_2-Mg_2NiH_4-$CeH_{2.73}/CeO_2$ nanocomposite with molar ratio of $CeH_{2.73}$ to CeO_2 of 1:1 during hydrogen desorption, *in situ* XRD measurements are carried out as shown in Figure 3b. Surprisingly, desorption of MgH_2 starts at almost the same temperature as Mg_2NiH_4. It indicates that the formation of symbiotic $CeH_{2.73}/CeO_2$ nanoparticles

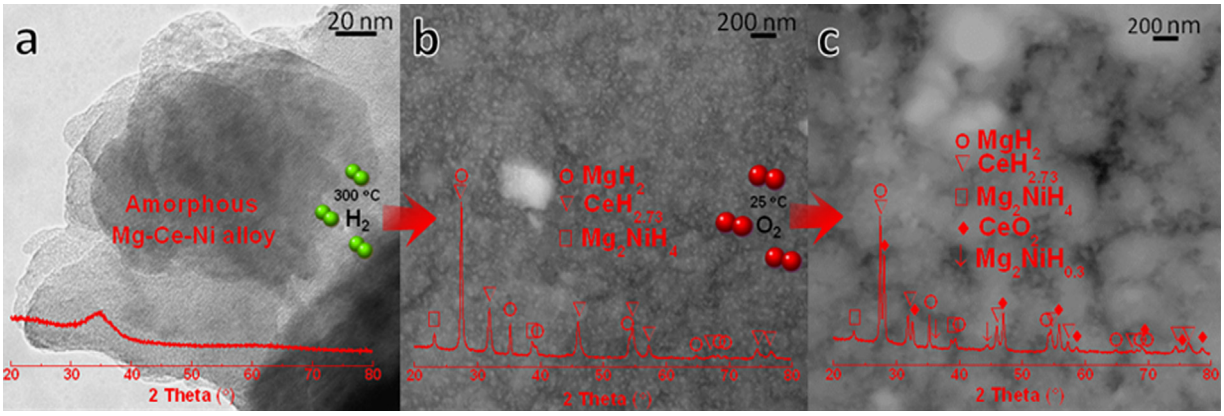

Figure 1 Materials fabrication. (a) TEM image of the amorphous Mg-Ce-Ni alloy, BSEM images of the amorphous alloy after (b) hydrogenation and then (c) oxidation treatments, the insets show the XRD patterns of the corresponding products.

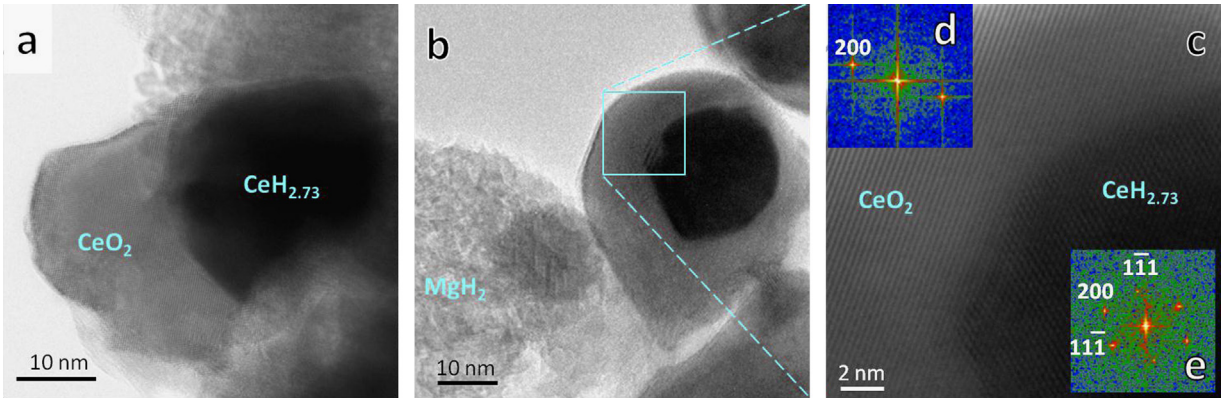

Figure 2 Microstructure characterizations. (a) HRTEM image of typical symbiotic $CeH_{2.73}/CeO_2$ nanoparticles. (b) TEM image of symbiotic $CeH_{2.73}/CeO_2$ nanoparticles with core–shell structure. (c) HRTEM image showing the magnified area in b. The insets are the corresponding FFT patterns of (d) the outer and (e) inner layers of the core–shell structure. Zoon axis [011].

remarkably reduces the desorption temperature of MgH_2, which is supposed to be higher than that of Mg_2NiH_4 where the thermodynamic stability is essentially lower [28]. Herein, DSC traces of the MgH_2–Mg_2NiH_4–$CeH_{2.73}$ and MgH_2–Mg_2NiH_4–$CeH_{2.73}/CeO_2$ composites are fitted with a Gaussian function based on the area ratio of MgH_2 to Mg_2NiH_4 of ~5:1 (Figure S4). As compared in Figure 3c, after oxidation treatment, desorption of MgH_2 divides into two stages and the onset desorption temperature is drastically reduced. The symbiotic $CeH_{2.73}/CeO_2$ nanoparticles have catalytic effect on dehydrogenations of both MgH_2 and Mg_2NiH_4, and higher catalysis on MgH_2 compared to Mg_2NiH_4. Under isothermal dehydrogenation kinetics measurements as given in the inset of Figure 3c, the dehydrogenation onset temperature of the MgH_2–Mg_2NiH_4–$CeH_{2.73}/CeO_2$ composite shows a decrease of ~80 and 150 °C compared with those of the MgH_2–Mg_2NiH_4–$CeH_{2.73}$ composite and pure MgH_2, respectively. The above results clearly demonstrate a significant improvement of catalyzing effect of the symbiotic $CeH_{2.73}/CeO_2$, compared with either $CeH_{2.73}$ or CeO_2 catalyst.

After dehydrogenation, the MgH_2–Mg_2NiH_4–$CeH_{2.73}/CeO_2$ nanocomposite with molar ratio of $CeH_{2.73}$ to CeO_2 of 1:1 decomposes into a composite consisting of Mg, Mg_2Ni, $CeH_{2.53}$, MgO and CeO_2 phases (Figure S5). Although $CeH_{2.73}$ (PDF 89-3694) and $CeH_{2.53}$ (PDF 39-0819) show quite similar XRD patterns, there are slight differences between them in high-angle ranges. We conclude that $CeH_{2.73}$ decomposes into $CeH_{2.53}$ after decomposition at 300 °C, similar results have also been reported by Yartys et al. [29]. The formation of small amount of MgO should be explained by the reaction between CeO_2 and MgH_2, which may create V_O (oxygen vacancy) in CeO_2 to enhance the desorption of H^- in MgH_2 [30]. However, the existence of sole CeO_2 could not display remarkably high catalytic activity, and the origin of the enhanced catalyzing effect based on the system of CeO_2 and $CeH_{2.73}$ hybrid needs to be further studied.

Therefore, we performed *in situ* TEM and HRTEM characterizations to make direct observations of the dehydrogenation process in the MgH_2–Mg_2NiH_4–$CeH_{2.73}/CeO_2$ nanocomposite with molar ratio of $CeH_{2.73}$ to CeO_2 of 1:1. Figure S6 shows the TEM images extracted from the *in situ* movie and the corresponding diffraction patterns during dehydrogenation. It can be clearly seen that the diffraction intensity of Mg increasingly enhances as desorption time prolongs, indicating the decomposition of MgH_2. The dynamic evolution of the interface structure of the symbiotic $CeH_{2.73}/CeO_2$ during dehydrogenation is studied *via in situ* HRTEM studies. Figure 4a presents the microstructural evolution of the typical symbiotic $CeH_{2.73}/CeO_2$ nanocrystals during dehydrogenation. Interestingly, the boundary region suffers severe distortions and the distorted area fluctuates wave-like during hydrogen desorption, suggesting that the interface region of the symbiotic nanocrystals undergoes structural evolution at atomic scale, which presumably plays a prominent role for hydrogen releasing in dehydrogenation. Detailed animation could refer to Supplementary Video S1. To further understand the evolution of interface and the origin of the intrinsic catalysis, theoretical calculations are performed to reveal the catalysis induced from the symbiotic $CeH_{2.73}/CeO_2$. Since the higher catalytic effect of the symbiotic $CeH_{2.73}/CeO_2$ on dehydrogenation of MgH_2 compared to that of Mg_2NiH_4, our calculations focus on the MgH_2–$CeH_{2.73}/CeO_2$, and the results are discussed in the following section.

Supplementary material related to this article can be found online at http://dx.doi.org/10.1016/j.nanoen.2014.06.026.

Theoretical calculations

We begin with the analysis of the formation energy of V_H in MgH_2, which could be significantly affected by the valence state variations (Figure S7a). The V_H is with the lowest formation energy of 1.35 eV among three vacancy types considered when the Fermi energy is around 3 eV. The formations of V_H^+ and V_H^- are more energetically favored than V_H when the Fermi energy ranges from 0 to 2.76 eV and from 3.08 to 4.5 eV respectively, indicating that the V_H valence state variations influence the V_H formation. The large areas of V_H^+ and V_H^- in Figure S7b indicate the energetic preference of high-concentration V_H formation. It has been reported that the V_O formation energy in CeO_2 could be reduced when there are empty orbitals lower than 4*f* of cerium [31]. For the MgH_2/CeO_2 interface, the Fermi

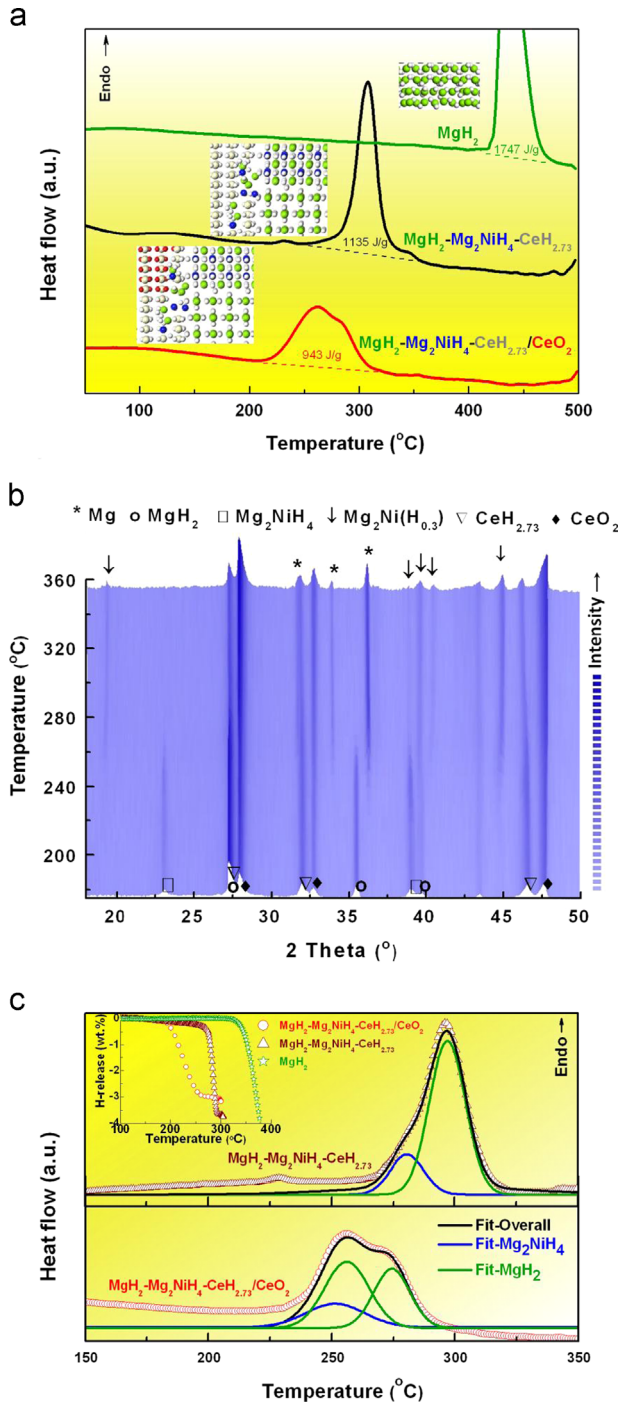

Figure 3 Hydrogen desorption. (a) DSC traces of pure MgH_2, the MgH_2-Mg_2NiH_4-$CeH_{2.73}$ nanocomposite and MgH_2-Mg_2NiH_4-$CeH_{2.73}/CeO_2$ nanocomposite with molar ratio of $CeH_{2.73}$ to CeO_2 of 1:1, heating rate of 10 K/min. The insets show the detailed atomic structures for each material. Magnesium, cerium, nickel, hydrogen and oxygen atoms are green, gray, blue, white and red, respectively. (b) *In situ* XRD patterns of the MgH_2-Mg_2NiH_4-$CeH_{2.73}/CeO_2$ nanocomposite with molar ratio of $CeH_{2.73}$ to CeO_2 is 1:1 during hydrogen desorption under Ar, heating rate of 2 K/min. (c) Comparison of DCS traces of the MgH_2-Mg_2NiH_4-$CeH_{2.73}$ and MgH_2-Mg_2NiH_4-$CeH_{2.73}/CeO_2$ nanocomposites are fitted *via* Gaussian function, the inset compares their TPD curves under initial pressure of 0.2 bar, heating rate of 2 K/min, pure MgH_2 is added as reference.

level of MgH_2 could be raised as oxygen vacancies often provide electrons to the Fermi sea of the system, leading to a much lower formation energy of V_H^-. Thus we suppose that hydrogen release would firstly happen in the MgH_2/CeO_2 interface and then hydrogen would migrate towards and across CeO_2 due to the role of CeO_2 as efficient vector for hydrogen diffusion [32].

We use the Climbing Image Nudged Elastic Band (CI-NEB [33,34]) to analyze the hydrogen migration barriers in three types of CeO_2, including pure CeO_2 (Type 1), CeO_2 with V_O (Type 2) and CeO_2 with V_O site partially occupied by hydrogen (Type 3), and the results are shown in Table S1. Figure 4b shows that the hydrogen migration in Type 1 is nearly barrierless (0.09 eV and 0.17 eV) since the hydrogen migration between 'hydroxyl' structures are quite easy [35]. We notice that the hydrogen migration could be remarkably influenced by V_O. Specifically, hydrogen migration near V_O might be attracted and tends to take up the V_O site with an energy barrier of 0.83 eV. The trap of hydrogen at V_O sites is locally stable since the energy barrier for hydrogen departure from the occupied V_O site is 1.09 eV. However, it does not affect the nearly barrierless migration of hydrogen in CeO_2 since the number of V_O is rather limited. In addition, we consider hydrogen migration barriers in two configurations of CeO_2 with V_O site partially occupied by hydrogen (c.f. Figure 4b). The formation energies of two structures are −0.36 eV and 0.69 eV. The large difference of formation energy of 1.05 eV indicates that the hydrogen 'dimer' structure is not energetically favored. In our NEB calculations, the hydrogen connected to H_{oc} (hydrogen at oxygen site) could depart spontaneously, which is manifested by the negative energy barrier, suggesting that the H_{oc} could not be able to trap hydrogen to form H-dimer. Furthermore, due to the limited concentration of H_{oc}, the dominating mechanism of hydrogen migrations in Type 3 is the same as in Type 1 where hydrogen migrates easily between 'hydroxyl' structures. In short, CeO_2 could serve as a good transporter for hydrogen migration.

Next, the formation energies of V_H in the CeH_x/CeO_2 (x=2, 2.25, 2.5, 2.75 and 3) interface region have been conducted to investigate the interfacial effects in comparison with the bulk cases. Although there are several possible configurations of the $CeH_{2.75}/CeO_2$ interface, we found that the $CeH_{2.75}/CeO_2$ interface would take an O-Ce-H configuration (Figure 4c) due to its lowest interfacial energy (−0.32 eV/Å^2) rather than the others, *i.e.* H-Ce-Ce-O (not stable) and Ce-O-H-Ce (−0.25 eV/Å^2). The O-Ce-H configuration is adopted in CeH_x/CeO_2 interfaces for comparison. Single and double V_H and V_O at different sites in the interface region are considered. Table S2 lists the formation energies of different types of V_H and V_O at the CeH_x/CeO_2 (x=2, 2.25, 2.5, 2.75 and 3) interfaces and in the bulk CeH_x (x=2.25, 2.5, 2.75 and 3). The formation energy of V_O at the $CeH_{2.75}/CeO_2$ interface is lowered to 2.06 eV compared to 2.91 eV in CeO_2 bulk, indicating that there might be the release of small amount of O_2 at the interface region (Figure S8). When x is less than 2.75, the formation of V_O becomes more difficult, which is reflected by the 2.89 eV of $CeH_{2.25}/CeO_2$ and 3.19 eV of $CeH_{2.5}/CeO_2$. Furthermore, the energetic advantage of V_O^{2nd} in three interfaces is in agreement with the previous papers [36,37], which proposed that the formation of V_O in second layer facilitates the atom

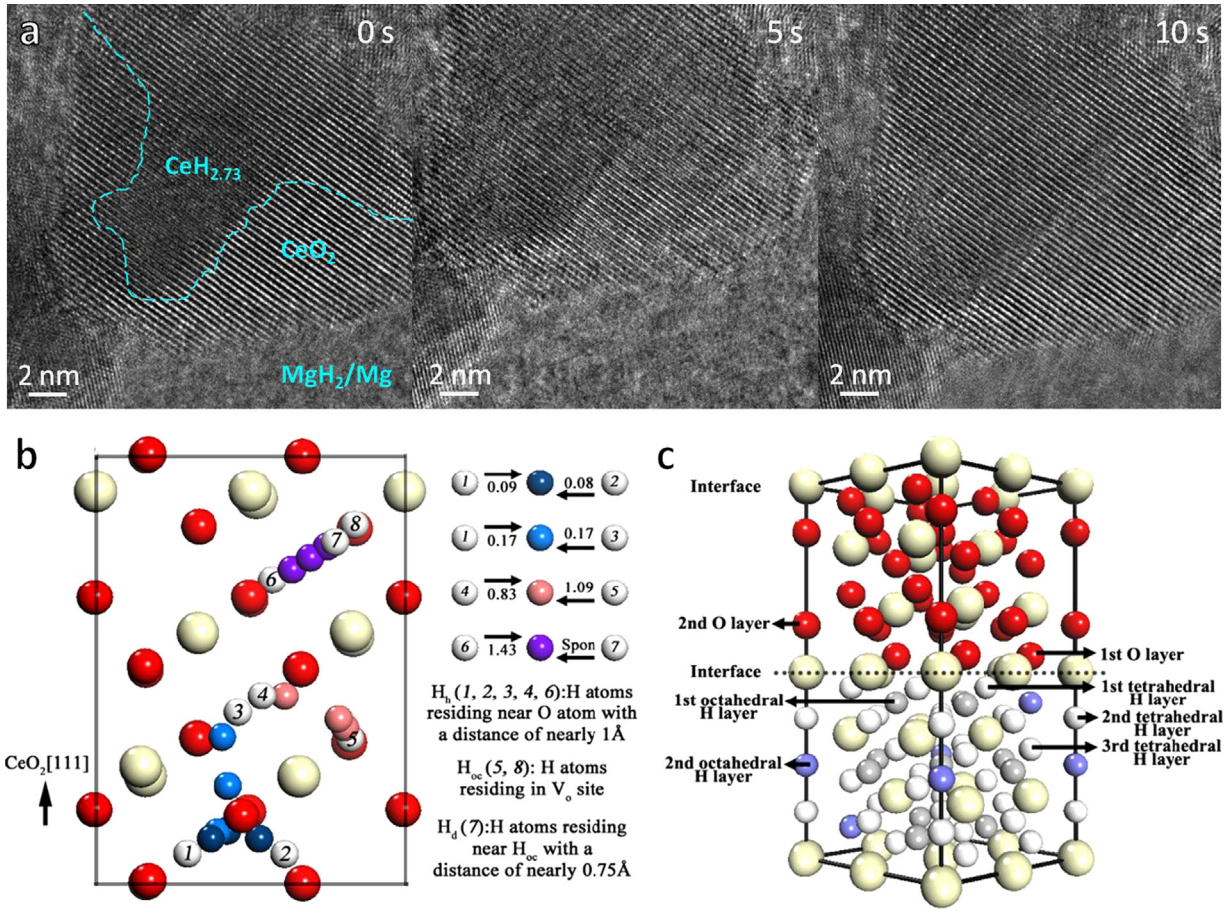

Figure 4 In situ dehydrogenation and theoretical calculations: (a) *In situ* HRTEM images of the dehydrogenation process, boundary between $CeH_{2.73}$ and CeO_2 is roughly drawn with a dash line at the beginning of hydrogen desorption. (b) Theoretical model and hydrogen migration barriers of CeO_2 bulk in side view. A ($2 \times 2 \times 1$) supercell consists of three layers of CeO_2(111) layers. Big beige balls represent cerium atoms while red balls denote oxygen atoms and the balls in other colors are hydrogen atoms. Three types of hydrogen atoms are considered, including the ones forming 'hydroxyl' structures (H_h), the ones occupying V_O sties (H_{oc}), and the ones forming hydrogen dimer with H_{oc} (H_d). Each NEB barrier is calculated independently. In the barrier calculations from Site 1 to Site 2 (from Site 2 to Site 1) and from Site 1 to Site 3, there is no V_O in CeO_2. In the barrier calculation from Site 4 to Site 5 and from Site 6 and Site 7, the oxygen atoms in Site 5 and Site 8 are vacant, respectively. (c) Theoretical model of $CeH_{2.75}/CeO_2$ interface in perspective view, corresponding to Table S2. A (2×2) superlattice model consisting of three layers of CeO_2(111) plus three layers of $CeH_{2.75}$(111). Big beige balls represent cerium atoms while red balls denote oxygen atoms and the balls in other colors are hydrogen atoms, respectively. Two types of hydrogen atoms, where the tetrahedral hydrogen in white and the octahedral hydrogen in gray and blue, coexist in CeH_3. The blue balls, which are supposed to exist in CeH_3 but not in $CeH_{2.75}$, are the missing atoms of the octahedral hydrogen layer. For CeH_2, there are only tetrahedral hydrogen atoms. Ordinal numbers denote the sequence of distances between vacancies and interface, from the closest to the furthest.

relaxations and electron localization that lead to system stability. The formation of V_O provides excess electrons which might facilitate the hydrogen desorption in MgH_2. The calculated CeH_3 bulk is found to exhibit a Ce-H_t (tetrahedral H) bond of 2.34 Å and a Ce-H_o (octahedral H) bond of 2.71 Å. The difference of the bond strength, which has also been observed in the lanthanum hydride [38], illuminates the possibility of easier H_o desorption due to the weaker Ce–H_o bonding. Our calculations of formation energies of V_H imply that the $CeH_{2.75}/CeO_2$ interface could be able to serve as an efficient "hydrogen pump". On one hand, the V_{Ho} at the $CeH_{2.75}/CeO_2$ interface is quite energetically unfavored. Specifically, single and double V_{Ho} are found to form spontaneously, reflected by negative formation energies even at the H-rich condition. The double vacancies $V_{Ho}^{1st}+V_{Ht}^{1st}$ and $V_{Ho}^{1st}+V_{Ht}^{2nd}$, which includes the concern of V_{Ho}, are also with low formation energies of 0.22 and 0.24 eV, respectively. On the other hand, the formation energies of single vacancy V_{Ht}^{1st} and V_{Ht}^{2nd} and double vacancies $V_{Ht}^{2nd}+V_{Ht}^{2nd}$ are in quite low level, namely 0.16, 0.17 and 0.06 eV, respectively, which might lead to an easy release of hydrogen as temperature increases. Moreover, the instability of CeH_3 indicates that it is difficult for hydrogen accumulation at the CeH_x/CeO_2 when x reaches 2.75. We attribute this to the instability of H_o of $CeH_{2.75}$ (the light gray atoms in Figure 4c). In contrast, the high stability of CeH_2, which arises from the stable bonding between cerium and H_t, implies that the hydrogen desorption at interface requires more energy as the hydrogen concentration is lowered. In the CeH_2/CeO_2,

$CeH_{2.25}/CeO_2$ and $CeH_{2.5}/CeO_2$ interfaces, the formation energies of V_H are all higher than those of the $CeH_{2.75}/CeO_2$ interface. Compared to the octahedral V_H formation energies in CeH_x bulk, the V_H formation energies at the $CeH_{2.75}/CeO_2$ interface are significantly decreased. In short, the interfacial effect of $CeH_{2.75}/CeO_2$ is capable of serving as an efficient "hydrogen pump" where excess hydrogen would be released very easily.

Conclusions

In summary, the hybrid of $CeH_{2.73}$ and CeO_2 with low catalytic effect exhibits surprisingly high catalytic activity for dehydrogenation of MgH_2. We show that the V_H formation in MgH_2 can be stimulated by electron transfer from CeO_2, and the CeO_2 is capable of transporting hydrogen to the $CeO_2/CeH_{2.73}$ interface where the release of hydrogen is quite easy. The spontaneous hydrogen release effect in the interface region of the symbiotic $CeO_2/CeH_{2.73}$ nanoparticles account for its role of efficient "hydrogen pump". The symbiotic $CeH_{2.73}/CeO_2$ catalyst is suitable for large-scale productions due to the easy fabrication technology. Our findings might open a novel approach to explore the advanced catalysts for alloy-based hydrogen storage materials.

Acknowledgments

This work was financially supported by the Ministry of Science and Technology of China (No. 2010CB631302), the National Natural Science Foundation of China (Nos. U1201241, 51071068 and 51271078) and KLGHEI (KLB11003) and the Fundamental Research Funds for the Central Universities.

Appendix A. Supporting information

Supplementary data associated with this article can be found in the online version at http://dx.doi.org/10.1016/j.nanoen.2014.06.026.

References

[1] A. Züttel, Mater. Today 6 (2003) 24–33.
[2] L. Schlapbach, A. Zuttel, Nature 414 (2001) 353–358.
[3] D. Pukazhselvan, V. Kumar, S.K. Singh, Nano Energy 1 (2012) 566–589.
[4] I.P. Jain, C. Lal, A. Jain, Int. J. Hydrog. Energy 35 (2010) 5133–5144.
[5] H. Shao, G. Xin, J. Zheng, X. Li, E. Akiba, Nano Energy 1 (2012) 590–601.
[6] G. Liang, J. Huot, S. Boily, A. Van Neste, R. Schulz, J. Alloys Compd. 292 (1999) 247–252.
[7] L.P. Ma, X.D. Kang, H.B. Dai, Y. Liang, Z.Z. Fang, P.J. Wang, P. Wang, H.M. Cheng, Acta Mater. 57 (2009) 2250–2258.
[8] J. Lu, Y.J. Choi, Z.Z. Fang, H.Y. Sohn, E. Rönnebro, J. Am. Chem. Soc. 132 (2010) 6616–6617.
[9] W. Oelerich, T. Klassen, R. Bormann, J. Alloys Compd. 315 (2001) 237–242.
[10] G. Barkhordarian, T. Klassen, R. Bormann, Scr. Mater. 49 (2003) 213–217.
[11] A.J. Du, S.C. Smith, X.D. Yao, G.Q. Lu, J. Am. Chem. Soc. 129 (2007) 10201–10204.
[12] L. Zaluski, A. Zaluska, P. Tessier, J.O. Strom-Olsen, R. Schulz, J. Alloys Compd. 217 (1995) 295–300.
[13] G. Barkhordarian, T. Klassen, R. Bormann, J. Phys. Chem. B 110 (2006) 11020–11024.
[14] J. Cui, H. Wang, J. Liu, L. Ouyang, Q. Zhang, D. Sun, X. Yao, M. Zhu, J. Mater. Chem. A 1 (2013) 5603–5611.
[15] S. Isobe, A. Ono, H. Yao, Y.M. Wang, N. Hashimoto, S. Ohnuki, Appl. Phys. Lett. 96 (2010) 223109–223111.
[16] C. Zlotea, F. Cuevas, J. Andrieux, C. Matei Ghimbeu, E. Leroy, E. Léonel, S. Sengmany, C. Vix-Guterl, R. Gadiou, T. Martens, M. Latroche, Nano Energy 2 (2013) 12–20.
[17] Y. Jia, L. Cheng, N. Pan, J. Zou, G. Lu, X. Yao, Adv. Energy Mater. 1 (2011) 387–393.
[18] H.J. Lin, W.H. Wang, M. Zhu, J. Non-Cryst. Solids 358 (2012) 1387–1390.
[19] H.J. Lin, L.Z. Ouyang, H. Wang, D.Q. Zhao, W.H. Wang, D.L. Sun, M. Zhu, Int. J. Hydrog. Energy 37 (2012) 14329–14335.
[20] G. Kresse, J. Hafner, Phys. Rev. B 47 (1993) 558–561.
[21] G. Kresse, J. Furthmuller, Comput. Mater. Sci. 6 (1996) 15–50.
[22] G. Kresse, J. Furthmüller, Phys. Rev. B 54 (1996) 11169–11186.
[23] J.P. Perdew, K. Burke, M. Ernzerhof, Phys. Rev. Lett. 77 (1996) 3865–3868.
[24] G. Kresse, D. Joubert, Phys. Rev. B 59 (1999) 1758–1775.
[25] S.L. Dudarev, G.A. Botton, S.Y. Savrasov, C.J. Humphreys, A.P. Sutton, Phys. Rev. B 57 (1998) 1505–1509.
[26] H.J. Monkhorst, J.D. Pack, Phys. Rev. B 13 (1976) 5188–5192.
[27] Database from HSC6.0 Software.
[28] J.J. Reilly, R.H. Wiswall, Inorg. Chem. 7 (1968) 2254–2256.
[29] V.A. Yartys, O. Gutfleisch, V.V. Panasyuk, I.R. Harris, J. Alloys Compd. 253–254 (1997) 128–133.
[30] V.E. Henrich, Rep. Prog. Phys. 48 (1985) 1481.
[31] O. Hellman, N.V. Skorodumova, S.I. Simak, Phys. Rev. Lett. 108 (2012) 135504.
[32] V. Sharma, P.A. Crozier, R. Sharma, J.B. Adams, Catal. Today 180 (2012) 2–8.
[33] G. Henkelman, B.P. Uberuaga, H. Jónsson, J. Chem. Phys. 113 (2000) 9901–9904.
[34] G. Henkelman, H. Jónsson, J. Chem. Phys. 113 (2000) 9978–9985.
[35] D. Marrocchelli, B. Yildiz, J. Phys. Chem. C 116 (2011) 2411–2424.
[36] M.V. Ganduglia-Pirovano, J.L.F. Da Silva, J. Sauer, Phys. Rev. Lett. 102 (2009) 026101.
[37] G.E. Murgida, M.V. Ganduglia-Pirovano, Phys. Rev. Lett. 110 (2013) 246101.
[38] T.C. Kerscher, G. Schöllhammer, P. Herzig, W. Wolf, R. Podloucky, S. Müller, Phys. Rev. B 86 (2012) 014107.

Huai-Jun Lin received his B.S. degree in Materials Science at South China University of Technology (SCUT) in 2009. He is now a Ph.D. candidate in School of Materials Science and Engineering, SCUT. He has been interested in Mg-based amorphous and nanocrystalline materials for hydrogen storage.

Jia-Jun Tang is now a Ph.D. candidate in School of Physics at South China University of Technology (SCUT). With the first-principles calculations, Tang is now mainly focusing on Mg hydrogen storage properties, including fundamental physics, interaction mechanism and real applications, *etc*. Specifically, Mg surface properties and interface physics are mainly focused on in Tang's researches, and the related papers are available online.

Qian Yu received her Ph.D. at University of California Berkeley in 2012, she is currently a post-doc at University of California Berkeley and Lawrence Berkeley National Laboratory. Dr. Yu has been interested in *in situ* transmission electron microscope characterization on materials properties.

Hui Wang received his B.S. degree in Metal Materials, Tianjin University in 1997, and Ph.D. degree in Material Science and Engineering, South China University of Technology (SCUT) in 2003. He is currently an associate professor in SCUT. His research focuses on hydrogen storage materials, microstructure analysis by X-ray diffraction with Rietveld method, non-equilibrium state synthesis of metastable materials *etc*.

Liu-Zhang Ouyang received his B.S. degree in Materials Science, Yanshan University in 1994, and Ph.D. degree in Material Science and Engineering, South China University of Technology (SCUT) in 2001. He is currently a professor in SCUT. His research focuses on hydrogen storage materials, hydrogen generation and lithium ion battery materials. He has published more than 100 papers in international journals.

Jiang-Wen Liu received his B.S. degree in Materials Science and Engineering, Shanghai Jiaotong University in 1987, and Ph.D. degree in Materials Science and Engineering, South China University of Technology (SCUT) in 1998. He is currently a professor in SCUT. His research focuses on nanomaterials and their nanostructure–property relationship through characterizing nanomaterials using electron microscopy, hydrogen storage materials, and lithium ion battery materials.

Wei-Hua Wang is a professor of Institute of Physics, Chinese Academy of Sciences at Beijing, China. His research focuses on the formation, structure, physical properties and glass transition in metallic glasses. He earned his Ph.D. degree in condensed matter physics at Chinese Academy of Sciences in 1993, and was Humboldt fellow in 1995–1997. He has published more than 100 papers in international journals.

Yu-Jun Zhao received his B.S. degree (1994) and Ph.D. degree (1999) in physics at Zhejiang University. Since then, he has been a post-doc at Northwestern University and National Renewable Energy Laboratory, and a researcher at Nanostellar Inc. at Silicon Valley. Dr. Zhao joined South China University of Technology (SCUT) in 2006 as a professor of physics, and is currently the group leader of Computational Physics for Condensed Matters at SCUT. Dr. Zhao has been interested in crystal defect theory and surface science, with research topics including magnetic semiconductors, surface catalysis, photovoltaic materials, and hydrogen storage materials.

Min Zhu is a professor in South China University of Technology (SCUT). He received his Ph.D. from Dalian University of Technology in 1988. He worked in the Technical University of Berlin as a Humboldt Research Fellow in 1993–1995. He was appointed as a “Cheung Kong Professor” in 2002. Prof. Zhu is working in the fields of hydrogen storage materials, lithium ion battery materials, shape memory alloys and mechanical alloying, and published more than 200 papers.